

# THE GEOMETRY OF POINT PARTICLES

Michael Atiyah <sup>†</sup> and Paul Sutcliffe <sup>‡</sup>

<sup>†</sup> *Department of Mathematics and Statistics,  
University of Edinburgh,  
King's Buildings, Edinburgh EH9 3JZ, U.K.  
Email : atiyah@maths.ed.ac.uk*

<sup>‡</sup> *Institute of Mathematics,  
University of Kent at Canterbury,  
Canterbury, CT2 7NZ, U.K.  
Email : P.M.Sutcliffe@ukc.ac.uk*

May 2001

## Abstract

There is a very natural map from the configuration space of  $n$  distinct points in Euclidean 3-space into the flag manifold  $U(n)/U(1)^n$ , which is compatible with the action of the symmetric group. The map is well-defined for all configurations of points provided a certain conjecture holds, for which we provide numerical evidence. We propose some additional conjectures, which imply the first, and test these numerically. Motivated by the above map, we define a geometrical multi-particle energy function and compute the energy minimizing configurations for up to 32 particles. These configurations comprise the vertices of polyhedral structures which are dual to those found in a number of complicated physical theories, such as Skyrmions and fullerenes. Comparisons with 2-particle and 3-particle energy functions are made. The planar restriction and the generalization to hyperbolic 3-space are also investigated.

# 1 Introduction

In their study of the spin-statistics theorem, Berry and Robbins [5] posed a very natural question in classical geometry concerning the existence of a symmetric map between two well-known spaces. The first space, denoted by  $\mathcal{C}_n(\mathbb{R}^3)$ , is the configuration space of  $n$  distinct ordered points in  $\mathbb{R}^3$ , and the second space is the flag manifold  $U(n)/U(1)^n$ , an element of which represents  $n$  orthonormal vectors in  $\mathbb{C}^n$ , each defined up to a phase. The Berry-Robbins problem is to construct, for each  $n$ , a continuous map

$$f_n : \mathcal{C}_n(\mathbb{R}^3) \mapsto U(n)/U(1)^n \quad (1.1)$$

compatible with the action of the symmetric group  $\Sigma_n$ , where this acts freely by permuting the points and the vectors respectively.

In the application of Berry and Robbins an element of  $\mathcal{C}_n(\mathbb{R}^3)$  represents the positions of  $n$  point particles and the matrix  $U(n)$  describes how a spin basis varies as the points move in space. In this approach to the spin-statistics theorem the Pauli sign associated with the exchange of particles arises as a geometric phase.

For the simplest case,  $n = 2$ , there is an obvious explicit map as noted by Berry and Robbins [5] but this construction is difficult to generalize to  $n > 2$ . A candidate solution for all  $n$  was first presented in [1], and is reviewed in Section 2. The map is only a candidate solution because it relies upon a certain non-degeneracy conjecture being true. Section 3 introduces an appropriate determinant function (whose non-vanishing describes the non-degeneracy) which can be used in subsequent quantitative investigations. In Section 4 we provide numerical evidence for the validity of this conjecture and propose and test numerically some additional conjectures, which imply the first.

Motivated by the construction of the above map, we define, in Section 5, a geometrical multi-particle energy function and compute the energy minimizing configurations for up to 32 particles. Remarkably, the resulting configurations of points comprise the vertices of polyhedral structures which are dual to those found in a number of complicated physical theories, including Skyrmions in nuclear physics and fullerenes in carbon chemistry. These results suggest a comparison, made in Section 6, with the historic problem concerning the minimal energy distribution of  $n$  point charges on the surface of a sphere, interacting via a 2-particle Coulomb force. In Section 7 we propose an approximation to our multi-particle energy function in terms of a 3-particle interaction, and find essentially the same minimal energy configurations.

The remaining sections concern minimal energy configurations in various modifications of the above picture. In Section 8 we enlarge the configuration space to consider unconstrained points in a product of spheres and show that the minimal energy configurations remain unchanged. In Section 9 we consider the restriction to points in the plane and repeat our earlier comparisons. Finally, in Section 10, we generalize the whole situation to hyperbolic 3-space.

## 2 The map

A candidate map for  $f_n$  in (1.1) was first presented in [1], to which we refer the reader for further details. Below we summarize the main ingredients.

First of all, any set of  $n$  linearly independent vectors in  $\mathbb{C}^n$  can be orthogonalized, in a way compatible with  $\Sigma_n$ , so the unitarity condition in (1.1) can be relaxed to require a map

$$F_n : \mathcal{C}_n(\mathbb{R}^3) \mapsto GL(n, \mathbb{C})/(\mathbb{C}^*)^n. \quad (2.1)$$

Given  $(\mathbf{x}_1, \dots, \mathbf{x}_n) \in \mathcal{C}_n(\mathbb{R}^3)$  then (2.1) is equivalent to defining  $n$  points  $p_i(\mathbf{x}_1, \dots, \mathbf{x}_n) \in \mathbb{CP}^{n-1}$ , for  $i = 1, \dots, n$ , which are linearly independent. We shall represent  $\mathbb{CP}^{n-1}$  via the space of polynomials of degree at most  $n-1$  in a Riemann sphere variable  $t \in \mathbb{CP}^1$ .

The explicit map is constructed as follows. For each pair  $i \neq j$  define the unit vector

$$\mathbf{v}_{ij} = \frac{\mathbf{x}_j - \mathbf{x}_i}{|\mathbf{x}_j - \mathbf{x}_i|} \quad (2.2)$$

giving the direction of the line joining  $\mathbf{x}_i$  to  $\mathbf{x}_j$ . Now let  $t_{ij} \in \mathbb{CP}^1$  be the point on the Riemann sphere associated with the unit vector  $\mathbf{v}_{ij}$ , via the identification  $\mathbb{CP}^1 \cong S^2$ , realized as stereographic projection. Finally, set  $p_i$  to be the polynomial in  $t$  with roots  $t_{ij}$  ( $j \neq i$ ), that is

$$p_i = \prod_{j \neq i} (t - t_{ij}). \quad (2.3)$$

The geometrical character of this construction means that, in addition to the required compatibility with  $\Sigma_n$ , the map is also compatible with rotations in  $\mathbb{R}^3$ , where  $SO(3)$  acts as the irreducible  $n$ -dimensional representation on the target space. Furthermore, the map is also translation and scale invariant; this follows trivially from (2.2).

The reason that this map is only a candidate solution is that the following conjecture must hold.

### Conjecture 1

For all  $(\mathbf{x}_1, \dots, \mathbf{x}_n) \in \mathcal{C}_n(\mathbb{R}^3)$  the polynomials  $p_1, \dots, p_n$  are linearly independent.

For  $n = 2$  this conjecture is trivially true and for  $n = 3$  it can be proved using simple geometry [1] or a direct algebraic computation [2], which we mention in the following section.

Note that an obvious case to check is that of  $n$  collinear points. Taking the line of collinear points to be in the direction given by  $t = \infty$  and ordering the  $\mathbf{x}_i$  in increasing distance along the line yields  $p_i = t^{i-1}$ , which are clearly independent.

For  $n > 3$  the conjecture remains open. In Section 4 we provide numerical evidence for this conjecture, and for some related conjectures which imply this one. Before this, we discuss a determinant function which will prove useful in making quantitative investigations, and which turns out to have independent interest, as we shall show. Because of this we shall treat it in greater generality than is needed for our immediate purposes. Readers

interested in the main results of our numerical calculations can skip the details of the next section.

### 3 Determinant functions

Linear independence can be characterized by the non-vanishing of the appropriate determinant. Because the polynomials  $p_1, \dots, p_n$  in conjecture 1 are only defined up to scalar factors we have to introduce an appropriate normalization if we want a definite determinant. There are several ways in which this can be done. One way is described in detail in [2]: for the absolute value of the determinant one just takes each  $p_i$  to have norm 1 and then takes the volume in  $\mathbb{C}^n$  given by the essentially unique  $SU(2)$ -invariant inner product. The phase requires more careful treatment as explained in [2]. There is however an alternative approach, which we shall adopt here, that has a number of advantages. On the one hand, as already exhibited in [2] this new definition has much better quantitative behaviour, and this we shall be exploiting in our numerical calculations. Another and apparently quite different advantage lies in the fact that this new definition extends naturally to hyperbolic 3-space and hence, on lines forecast in [2], to Minkowski space.

We start as follows. Consider  $n(n-1)$  variables  $u_{ij} \in \mathbb{C}^2$  ( $i \neq j$ )  $i, j = 1, 2, \dots, n$ , and form the  $n$  ‘polynomials’  $p_1, \dots, p_n$  given by

$$p_i = \prod_{j \neq i} u_{ij}. \quad (3.1)$$

This is a more abstract version of (2.3), where  $u_{ij}$  is regarded as a linear form

$$u_{ij} = a_{ij}t_0 + b_{ij}t_1 \quad (3.2)$$

in two homogeneous coordinates  $(t_0, t_1)$  related to the inhomogeneous coordinate  $t$  of (2.3) by  $t = t_0/t_1$ .

If we want to avoid using coordinates, and hence emphasize the invariance, we consider  $\mathbb{C}^2$  as a vector space with a skew non-degenerate form  $(u, v)$ . In particular this identifies  $\mathbb{C}^2$  with its dual, the space of linear forms. Note that  $\mathbb{C}^2$  is the space of *spinors*.

In (3.1)  $p_i$  is just given by the symmetrized tensor product of  $n$  copies of  $\mathbb{C}^2$

$$S^n(\mathbb{C}^2) \cong \mathbb{C}^n. \quad (3.3)$$

Since  $SL(2, \mathbb{C})$  acts on  $\mathbb{C}^2$  preserving the skew-form it acts (irreducibly) on  $\mathbb{C}^n$  via  $SL(n, \mathbb{C})$ .

Now take the  $n$  vectors  $p_1, \dots, p_n$  in  $\mathbb{C}^n$  and form the exterior product

$$\omega = p_1 \wedge p_2 \wedge \dots \wedge p_n \quad (3.4)$$

which is an element of the  $n$ th exterior power of  $\mathbb{C}^n$ . Since there is a canonical isomorphism

$$\Lambda^n(\mathbb{C}^n) \cong \mathbb{C} \quad (3.5)$$

$\omega$  is essentially a complex number. More precisely

$$\omega = \varphi e_1 \wedge e_2 \wedge \dots \wedge e_n \quad (3.6)$$

where  $e_i$  is the monic polynomial  $t^{i-1}$ , or in other words  $\varphi$  is the determinant of the matrix of coefficients of the polynomials  $p_1, \dots, p_n$ . Our parameter  $t$  is assumed here to come from an orthogonal, or at least symplectic basis  $(t_0, t_1)$  of  $\mathbb{C}^2$  (see the later discussion of symplectic representatives).

We have therefore defined a *complex-valued function*  $\varphi(u_{ij})$ . It has the following properties

- (1)  $\varphi$  is invariant under the action of  $SL(2, \mathbb{C})$  on the  $u_{ij}$ .
- (2)  $\varphi(u_{ij}^*) = \overline{\varphi(u_{ij})}$ , where  $(a + bt)^* = (-\bar{b} + \bar{a}t)$ .
- (3)  $\varphi(u_{\sigma(i)\sigma(j)}) = \text{sign}(\sigma)\varphi(u_{ij})$ , for any permutation  $\sigma$  of  $(1, \dots, n)$ .
- (4)  $\varphi$  is a multi-linear function of the  $u_{ij}$ .
- (5) For  $n = 2$ ,  $\varphi = (u_{12}, u_{21})$ .

Remark: The essential difference between this definition and the earlier one in [2] is that here we do not use any Hermitian metric on  $\mathbb{C}^n$ , only the volume form. That is why we have the larger symplectic group  $SL(2, \mathbb{C})$  rather than just  $SU(2)$ .

In terms of  $\varphi$  we can proceed to define a sequence of related functions  $\varphi_k$  (for  $2 \leq k < n$ ), using subsets  $I$  of  $(1, \dots, n)$  of length  $|I| = k$ . For each such  $I$  let  $\varphi_I$  be the function  $\varphi$  applied to the variables  $u_{ij}$  with  $i, j \in I$ , and then put

$$\varphi_k = \prod_I \varphi_I, \quad |I| = k. \quad (3.7)$$

Thus we have the sequence of functions

$$\varphi = \varphi_n, \varphi_{n-1}, \dots, \varphi_2. \quad (3.8)$$

Clearly from property (4) of  $\varphi$  we deduce

- (6)  $\varphi_k$  is homogeneous in each  $u_{ij}$  of degree  $\binom{n-2}{k-2}$ .

If we take a ratio of appropriate powers of the  $\varphi_k$  then we will get a rational function of homogeneity zero in the  $u_{ij}$ . This means that it is a rational function of the corresponding points  $t_{ij} \in P_1(\mathbb{C})$ . In particular we shall be interested in

$$D(t_{ij}) = \varphi_n(u_{ij})/\varphi_2(u_{ij}). \quad (3.9)$$

Note that this has poles only where  $\varphi_2(u_{ij}) = 0$ , ie. where  $u_{ij}$  and  $u_{ji}$  are proportional, or equivalently where  $t_{ij} = t_{ji}$ . From now on we restrict ourselves to the subspace of the variables where, for all  $i, j$ ,  $t_{ij} \neq t_{ji}$ .

A convenient way to make the definition of  $D$  more explicit is to use *symplectic representatives* for the  $u_{ij}$ . By definition this means that we choose each pair  $u_{ij}, u_{ji}$  so that (for  $i < j$ )

$$(u_{ij}, u_{ji}) = 1. \quad (3.10)$$

This makes  $\varphi_2 = 1$  and so  $D = \varphi$  is just the determinant of the coefficients of the polynomials  $p_1, \dots, p_n$ .

If we introduce a Hermitian metric on  $\mathbb{C}^2$ , with  $SU(2)$  now being the symmetry group we can introduce the anti-podal map

$$t \mapsto t^* = -\bar{t}^{-1} \quad (3.11)$$

and we can lift this to an anti-linear map  $u \mapsto u^*$  on  $\mathbb{C}^2$ . Explicitly, in terms of a standard basis, this is (as in (2) above)  $(a, b) \mapsto (-\bar{b}, \bar{a})$ . If we think of  $\mathbb{C}^2$  as the quaternions then  $u^* = u j$ . Note that

$$(u, u^*) = |a|^2 + |b|^2 = |u|^2 \quad (3.12)$$

so that if  $|u| = 1$ , the pair  $u, u^*$  are a symplectic pair. Such a pair we shall briefly refer to as an orthogonal pair (since  $|u| = |u^*| = 1, \langle u, u^* \rangle = 0$ ).

We are now ready to return to our configurations of points  $\mathbf{x}_1, \dots, \mathbf{x}_n$  in  $\mathbb{R}^3$  and the corresponding points  $t_{ij}$  (or  $\mathbf{v}_{ij}$ ) given by (2.2), ie. by the directions of the vectors  $\mathbf{x}_j - \mathbf{x}_i$ . Our function  $D(t_{ij})$  then gives rise to a function  $D(\mathbf{x}_i)$  on  $\mathcal{C}_n(\mathbb{R}^3)$ . Since our  $t_{ij}$  now satisfy  $t_{ij} = t_{ji}^*$  we can choose orthogonal representatives for the  $u_{ij}$  and so we get  $D$  as the determinant of the coefficients of the polynomials  $p_1, \dots, p_n$ .

In [2] we defined  $D$  explicitly in this way, except that we multiplied it by a numerical coefficient  $\mu(n)$ . This arose from using the invariant inner product on  $\mathbb{C}^n$ , but is not natural from our present more invariant point of view. We have therefore dropped it. Note however that the geometrical considerations in [2] led to an upper bound for  $|D|$ , which now becomes

$$|D| \leq \mu(n)^{-1} = \left\{ \prod_{s=0}^{n-1} \binom{n-1}{s} \right\}^{1/2} \quad (3.13)$$

where  $\binom{n-1}{s}$  is the binomial coefficient.

The whole purpose of introducing our function  $D$  is of course that conjecture 1 is equivalent to

$$D(\mathbf{x}_1, \dots, \mathbf{x}_n) \neq 0. \quad (3.14)$$

Properties (1) and (2) show that, as a function  $\mathcal{C}_n(\mathbb{R}^3) \mapsto \mathbb{C}$  it is covariant with respect to the full Euclidean group of  $\mathbb{R}^3$ , with reflections acting as complex conjugation on  $\mathbb{C}$ . This implies in particular that  $D$  is *real* for any *planar* configuration, which is automatic for  $n = 2$  ( $D = 1$ ) and  $n = 3$ . In general, for  $n \geq 4$ ,  $D$  is complex and we shall introduce its norm

$$V = |D| \quad (3.15)$$

as a real-valued function on  $\mathcal{C}_n(\mathbb{R}^3)$  and refer to it briefly as the *volume*. For any collinear set we have already noted that, in a suitable orientation, we have  $p_i = t^{i-1}$  and so  $V = 1$ .

For  $n = 3$  the calculation of the volume yields a nice geometrical answer [2]. Let the triangle formed by the three points  $\mathbf{x}_1, \mathbf{x}_2, \mathbf{x}_3$  have angles  $\theta_1, \theta_2, \theta_3$ , then

$$V = \frac{1}{2}[\sin^2\left(\frac{\theta_1 + \theta_2}{2}\right) + \sin^2\left(\frac{\theta_2 + \theta_3}{2}\right) + \sin^2\left(\frac{\theta_3 + \theta_1}{2}\right)]. \quad (3.16)$$

This formula is obtained by explicitly computing the polynomials  $p_i$  and using some elementary geometry.

Using the fact that  $\sum_{i=1}^3 \theta_i = \pi$  the critical points of  $V$  are easily determined as the solutions of

$$\sin \theta_1 = \sin \theta_2 = \sin \theta_3. \quad (3.17)$$

There are two classes of solutions. The first is  $\theta_1 = \theta_2 = 0$  and  $\theta_3 = \pi$ , in which the triangle degenerates to three collinear points with  $V = 1$ . This is the global minimum of the volume. The second is the global maximum, given by the equilateral triangle  $\theta_1 = \theta_2 = \theta_3 = \pi/3$ , for which  $V = 9/8$ . Thus,  $V$  is non-zero for all configurations of three points and conjecture 1 is proved in the case  $n = 3$ .

For  $n > 3$  conjecture 1 has yet to be proved. In the following section we make use of the volume function  $V$  to provide numerical evidence for this conjecture, and for some related conjectures which imply this one.

## 4 Conjectures and tests

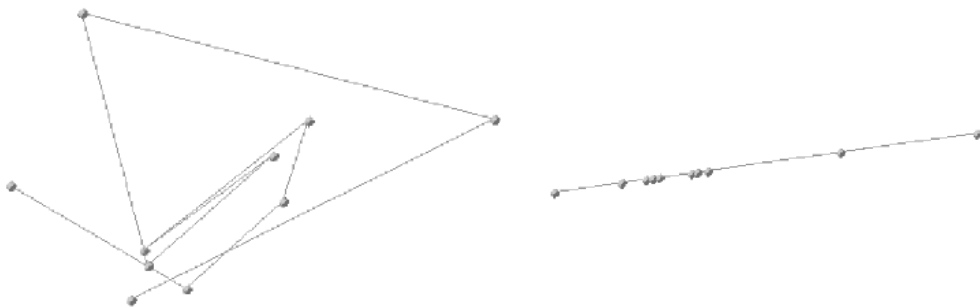


Figure 1: An initial random configuration of ten points is shown in the left-hand plot, with lines connecting consecutive points to aid visualization. The right-hand plot is the end result of applying the annealing process to minimize the volume, resulting in ten collinear points.

The calculations of the previous section prove that  $V \geq 1$  for  $n = 2$  and  $n = 3$ . Furthermore, we have seen that for  $n$  collinear points,  $V = 1$ . This prompts us to make the following slightly stronger conjecture.

### Conjecture 2

For all  $(\mathbf{x}_1, \dots, \mathbf{x}_n) \in \mathcal{C}_n(\mathbb{R}^3)$ , the volume satisfies  $V \geq 1$ .

Note that conjecture 2 implies conjecture 1, since this only required that  $V$  be non-zero. However the numerical evidence we provide below is all consistent with the stronger conjecture 2.

In order to test conjecture 2 we apply a numerical minimization algorithm known as simulated annealing [13] to search the configuration space of  $n$  points for the minimum value of the function  $V$ . In each case we perform several annealing runs with the initial conditions generated by assigning random positions to each of the  $n$  points. We have applied this procedure for all  $n \leq 20$  and in each case the end result of the annealing process is a collinear set of points with the associated volume  $V = 1$ , to a high precision. As an example we display in fig. 1 the initial and final configurations of points for a typical annealing run with  $n = 10$ . The initial volume has the value  $V = 187.07..$ , and at the end of the annealing process this has reduced to  $V = 1.00000..$ , with the associated points being collinear. We believe that this evidence for the conjecture is quite convincing.

One obvious line of attack for proving conjecture 2 would be to attempt some form of proof by induction, since we already know that this conjecture holds for  $n = 2$  and  $n = 3$ . As a move in this direction we propose a further conjecture.

To state this recall the sequence of functions  $\varphi_k$  we introduced in (3.8). We noted that the ratios of appropriate powers of the  $\varphi_k$  would be functions of the  $t_{ij}$  (and hence functions on  $\mathcal{C}_n(\mathbb{R}^3)$ ) and we defined  $D$  by (3.8) as the ratio of  $\varphi_n$  to  $\varphi_2$ , and equal to  $\varphi_n$  in the symplectic normalization which makes  $\varphi_2 = 1$ . Since  $\varphi_{n-1}$  has homogeneity  $(n-2)$  (property (6)) we can also consider

$$\varphi^{n-2}/\varphi_{n-1}. \quad (4.1)$$

This can also be rewritten as

$$D^{n-2}/\prod_{i=1}^n D_i \quad (4.2)$$

where  $D_i$  is the function  $D$  evaluated on the configuration obtained by omitting  $\mathbf{x}_i$ . In terms of absolute values this gives the function (with  $V_i = |D_i|$ )

$$\chi = \frac{V^{n-2}}{\prod_{i=1}^n V_i}. \quad (4.3)$$

Our third conjecture can now be stated.

### Conjecture 3

Let  $V$  denote the volume for  $n$  points,  $(\mathbf{x}_1, \dots, \mathbf{x}_n) \in \mathcal{C}_n(\mathbb{R}^3)$ , and let  $V_i$  denote the volume for the  $n - 1$  points  $(\mathbf{x}_1, \dots, \mathbf{x}_{i-1}, \mathbf{x}_{i+1}, \dots, \mathbf{x}_n) \in \mathcal{C}_{n-1}(\mathbb{R}^3)$ , obtained by deleting the point  $\mathbf{x}_i$ . Then, for all  $(\mathbf{x}_1, \dots, \mathbf{x}_n) \in \mathcal{C}_n(\mathbb{R}^3)$ ,

$$V^{n-2} \geq \prod_{i=1}^n V_i. \quad (4.4)$$

Conjecture 3, applied inductively, eventually shows that a power of  $V$  is bounded below by the product of volumes over all pairs  $(\mathbf{x}_i, \mathbf{x}_j)$  and this is just 1. Thus conjecture 3 implies conjecture 2. In terms of the sequence  $\varphi_k$  conjecture 3 asserts that, for the products of the appropriate powers, we get a descending sequence of values, beginning with  $V$  and ending with 1.

We have obtained similar numerical evidence for conjecture 3 as we did for conjecture 2, by applying our simulated annealing algorithm to the function  $\chi$  defined by (4.3). Again this results in a set of collinear points, for which  $\chi = 1$  to a high precision and the inequality (4.4) becomes an equality.

## 5 Minimal energy configurations

In this section we investigate the configurations of points for which the volume  $V$  is maximal. For this purpose it is convenient to introduce the energy function

$$E = -\log V \quad (5.1)$$

so that the critical points we seek are the minimizers of this energy. This is quite a natural definition of the energy in that, if we consider two well-separated clusters, then the volume factorizes and so the total energy is the sum of the energies of the two non-interacting clusters. In fact the deviation from the sum is of order  $1/r$ , where  $r$  is the ratio of the separation to the cluster scale, but there is also an angular dependence.

We see that in our geometrical investigations of point configurations or ‘particles’ we have been led to an interesting multi-particle energy function which places a penalty on compressing the associated volume form. We shall now investigate the minimal energy arrangements of points. Note that the upper bound (3.13) for  $|D|$  gives a lower bound for the energy  $E$ .

Note that conjecture 2 is equivalent to the statement that the energy is non-positive,  $E \leq 0$ , whereas conjecture 1 merely implies that the energy is finite.

For two points, the energy is independent of the positions of the points, it being identically zero, so there is no 2-particle interaction energy.

For three points, we have already seen that the minimal energy configuration is an equilateral triangle (with arbitrary scale, location and orientation) and the energy is  $E = -\log(9/8) = -0.11778\dots$

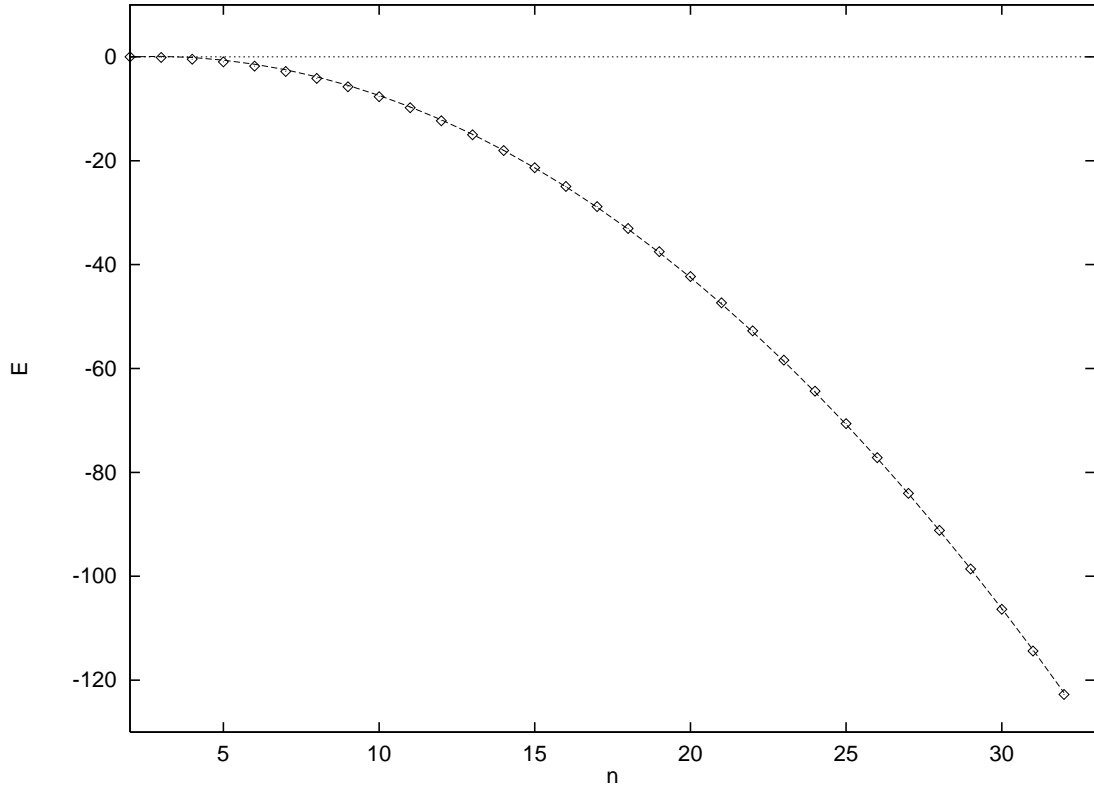


Figure 2: The energy  $E$  (diamonds) of the minimizing configuration for  $n$  points with  $2 \leq n \leq 32$ . The dashed curve represents the quadratic fit described in the text.

We now apply our simulated annealing algorithm to the energy function (5.1) to determine the structures for larger  $n$  which generalize the equilateral triangle at  $n = 3$ .

In fig. 2 we plot (diamonds) the minimum value of the energy for  $2 \leq n \leq 32$ . The precise values are listed in the second column of table 1. The dashed curve in fig. 2 is the result of a least squares fit to the data using the quadratic approximation

$$E(n) = -an^2 + bn + 4a - 2b \quad (5.2)$$

where the constant term has been chosen so that  $E(2) = 0$ , in agreement with the result that the energy of any two points is zero. The values obtained by fitting to the data are  $a = 0.143$  and  $b = 0.792$ . As can be seen from the plot, this approximation is fairly accurate, and it would be nice to have some understanding of this quadratic growth.

Related to this last issue, note that conjecture 3 corresponds to an upper bound for the  $n$ -particle energy in terms of the  $(n - 1)$ -particle energy. Explicitly,

$$E \leq \frac{1}{n-2} \sum_{i=1}^n E_i \quad (5.3)$$

where  $E_i$  denotes the energy when the point  $\mathbf{x}_i$  is removed. If we denote by  $B_{n-1}$  an upper bound for the  $(n-1)$ -particle energy then (5.3) implies that we may take  $B_n = \frac{n}{n-2} B_{n-1}$  as an upper bound for the  $n$ -particle energy. Iterating this relation up from the 2-particle energy just reproduces the result that the energy is non-positive but iterating up from the 3-particle energy yields

$$B_n = \frac{-n(n-1)}{6} \log(9/8) \quad (5.4)$$

for  $n \geq 3$ . Although the numerical values in the upper bound (5.4) are poor in comparison with the fit (5.2), the quadratic growth, damped by a linear factor, is reproduced.

In the third column of table 1 we present the symmetry group of the energy minimizing configuration and in fig. 3 we display polyhedra whose vertices consist of the  $n$  points of this configuration. The views in fig. 3 are down the main symmetry axis and the corresponding views up the main symmetry axis are presented in fig. 4

In case the reader is not familiar with the notation used for point group symmetries we briefly recount the main details here. The Platonic groups are the rotational symmetries of the tetrahedron ( $T$ ), the octahedron/cube ( $O$ ) and the icosahedron/dodecahedron ( $Y$ ). The dihedral group  $D_n$  is obtained from the cyclic group of order  $n$ ,  $C_n$ , by the addition of a  $C_2$  axis which is orthogonal to the main  $C_n$  symmetry axis. The group  $D_n$  can be extended by the addition of a reflection symmetry in two ways: by including a reflection in the plane perpendicular to the main  $C_n$  axis, which produces the group  $D_{nh}$  or, alternatively, a reflection symmetry may be imposed in a plane which contains the main symmetry axis and bisects the  $C_2$  axes, which results in the group  $D_{nd}$ . In the same way as for the dihedral groups the Platonic groups may also be enhanced by reflection symmetries, again denoted by the subscripts  $h, d$ . The addition of a subscript  $h$  to a cyclic group denotes a horizontal reflection symmetry, but a vertical reflection plane is denoted by a subscript  $v$ .

We find that in all the above minimizing configurations the points lie on, or very close to, the surface of a sphere. To measure the deformation from a spherical arrangement we compute the following quantity  $\delta$ . First of all, we compute the centre of mass of the configuration  $\mathbf{X} = \frac{1}{n} \sum_{i=1}^n \mathbf{x}_i$  and use the translational invariance of the problem to position this at the origin. Next we use the scale invariance to rescale the position vectors of all the points (by the same amount) so that the point (or points) which is furthest from the origin lies on the unit sphere.  $\delta$  is then defined as the distance from the origin of the point which is closest to the origin. Clearly from this definition  $\delta \leq 1$ , with equality if and only if all  $n$  points lie on the unit sphere (after we have made the above transformations). The computed value of  $\delta$  is given in the fourth column of table 1. In each case  $\delta$  is very close to unity, the greatest deviation occurring for  $n = 5$  and  $n = 7$  where  $\delta = 0.97$ , which is still quite close to a spherical arrangement. In order to accurately compute  $\delta$  the minimum energy needs to be calculated to a high precision, but we believe that the results for  $\delta$  quoted to two decimal places in the fourth column of table 1 are accurate to this level. As an example, the  $n = 5$  polyhedron is a trigonal bipyramidal composed of a point at each of the north and south poles of the unit sphere and an equilateral triangle in the equatorial plane but on a circle of radius 0.97. If we rescale the equilateral triangle so that all five points lie on the unit sphere then the energy increases from  $E = -0.9718$  to  $E = -0.9714$ ,

$n$	$E$	$G$	$\delta$	$E_\Delta$	$\tilde{E}$	$\tilde{\delta}$
2	0.0000	$D_{\infty h}$	1.00	-	-	-
3	-0.1178	$D_{3h}$	1.00	-0.1178	-0.1178	1.00
4	-0.4463	$T_d$	1.00	-0.1178	-0.4463	1.00
5	-0.9718	$D_{3h}$	0.97	-0.1086	-0.9708	0.98
6	-1.7994	$O_h$	1.00	-0.1062	-1.7994	1.00
7	-2.8262	$D_{5h}$	0.97	-0.1018	-2.8226	0.98
8	-4.1632	$D_{4d}$	1.00	-0.0997	-4.1627	1.00
9	-5.7746	$D_{3h}$	0.99	-0.0978	-5.7743	0.99
10	-7.6597	$D_{4d}$	0.99	-0.0962	-7.6591	1.00
11	-9.8001	$C_{2v}$	0.98	-0.0947	-9.7985	0.99
12	-12.3165	$Y_h$	1.00	-0.0939	-12.3165	1.00
13	-15.0021	$C_{2v}$	0.99	-0.0927	-15.0010	0.99
14	-18.0354	$D_{6d}$	0.99	-0.0919	-18.0334	0.99
15	-21.3443	$D_3$	0.99	-0.0912	-21.3427	1.00
16	-24.9525	$T$	1.00	-0.0906	-24.9498	1.00
17	-28.8498	$D_{5h}$	1.00	-0.0900	-28.8498	1.00
18	-33.0439	$D_{4d}$	1.00	-0.0895	-33.0438	1.00
19	-37.5018	$C_{2v}$	1.00	-0.0890	-37.4987	1.00
20	-42.3013	$D_{3h}$	1.00	-0.0886	-42.3005	1.00
21	-47.3714	$C_{2v}$	1.00	-0.0882	-47.3714	1.00
22	-52.7464	$T_d$	1.00	-0.0879	-52.7461	1.00
23	-58.3834	$D_3$	1.00	-0.0876	-58.3820	1.00
24	-64.3697	$O$	1.00	-0.0873	-64.3694	1.00
25	-70.6018	$C_{1h}$	1.00	-0.0870	-70.6010	1.00
26	-77.1541	$C_2$	1.00	-0.0867	-77.1541	1.00
27	-84.0314	$D_{5h}$	1.00	-0.0865	-84.0314	1.00
28	-91.1685	$T$	1.00	-0.0863	-91.1685	1.00
29	-98.5921	$D_3$	1.00	-0.0861	-98.5915	1.00
30	-106.3488	$D_2$	1.00	-0.0859	-106.3488	1.00
31	-114.3918	$C_{3v}$	1.00	-0.0857	-114.3917	1.00
32	-122.7781	$Y_h$	1.00	-0.0855	-122.7781	1.00

Table 1: For  $2 \leq n \leq 32$  we list the energy,  $E$ , of the minimizing configuration, its symmetry group,  $G$ , and the deformation,  $\delta$ , from a spherical arrangement.  $E_\Delta$  is the minimized average 3-particle energy (described later), and  $\tilde{E}, \tilde{\delta}$  are the values of  $E, \delta$  computed from the 3-particle energy minimizing configurations.

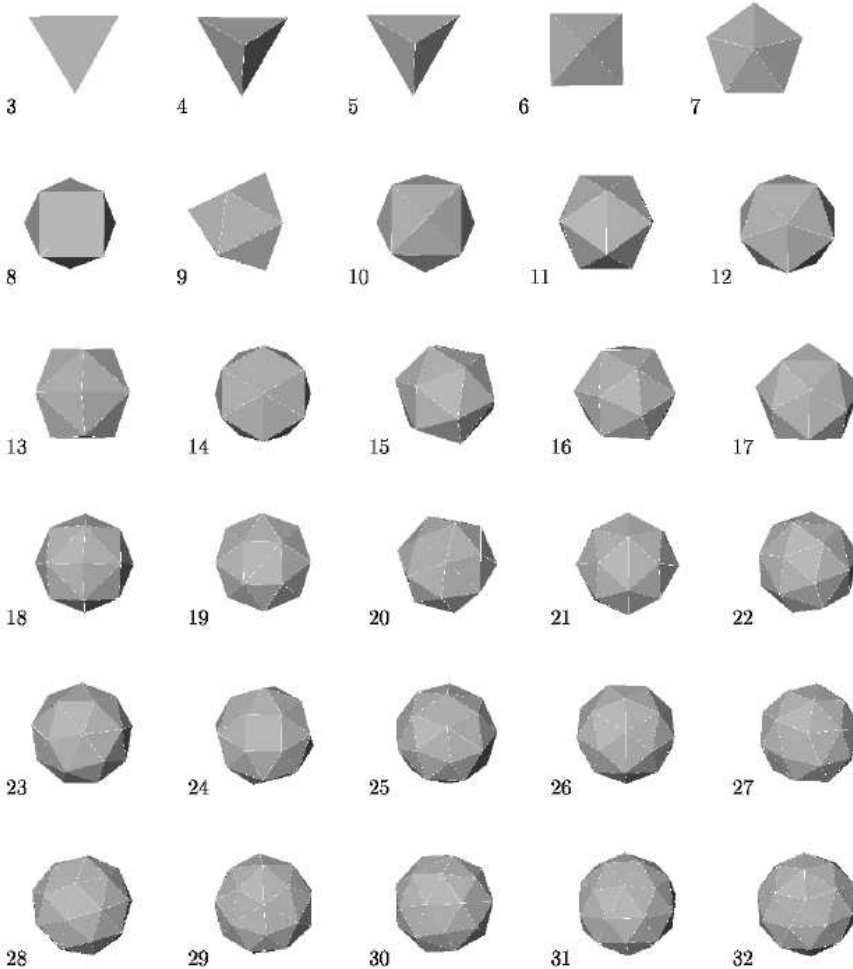


Figure 3: View down the main symmetry axis of the polyhedra associated with the energy minimizing configurations for  $3 \leq n \leq 32$ .

indicating that the non-spherical arrangement is the correct minimum of the energy. For  $n = 7$  the situation is similar, with the polyhedron being a pentagonal bipyramid, but this time it is the two points at the poles which are inside the unit sphere when the pentagon is scaled so that its vertices lie on the equator of the unit sphere. Again rescaling to a spherical arrangement slightly increases the energy from  $E = -2.8262$  to  $E = -2.8255$ .

It is perhaps useful to briefly describe the salient features of the polyhedra we have found. For  $n = 4, 6, 12$  the polyhedra are the Platonic solids, namely the tetrahedron, octahedron and icosahedron, respectively. For  $n = 5$  and  $n = 7$ , we have already mentioned that the trigonal and pentagonal bipyramids are formed. Note that the  $n = 6$  case also fits in the middle of this pair, since the octahedron may be thought of as a special case of the square bipyramid.  $n = 8$  is the first example in which some of the faces are not triangular,

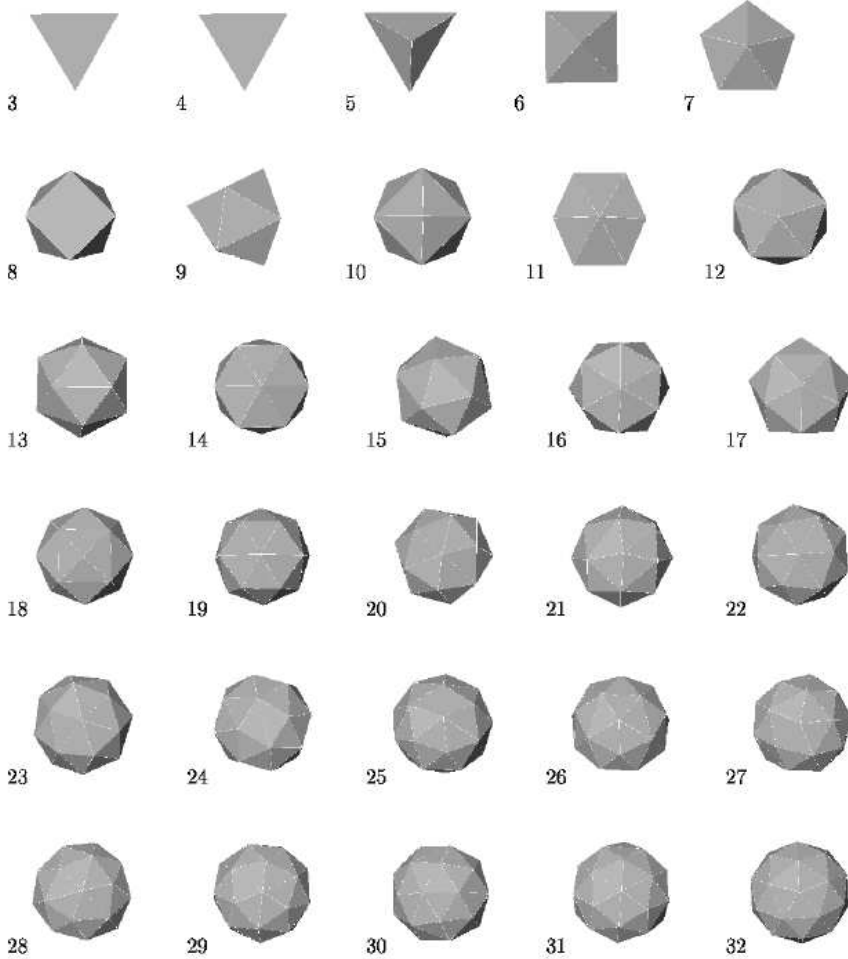


Figure 4: View up the main symmetry axis of the polyhedra associated with the energy minimizing configurations for  $3 \leq n \leq 32$ .

it being a square anti-prism, obtained from a cube by rotating the top face by  $45^\circ$  relative to the bottom face. This example demonstrates a general feature that the most symmetric configurations are not automatically those of lowest energy. Nine points lie on the vertices of three parallel equilateral triangles, with the middle triangle rotated by  $60^\circ$  relative to the other two. The  $n = 10$  polyhedron can be obtained from the  $n = 8$  one by replacing each square by a hat made from four triangles with a tetravalent vertex. The first polyhedron containing a hexamer (a vertex with six nearest neighbours) occurs at  $n = 11$ . There are two tetravalent vertices and the remaining eight are pentamers (vertices with five nearest neighbours). The existence of the single hexamer clearly forbids the solution from having much symmetry. Another general pattern is that if the number of points is one more or less than an exceptionally symmetric configuration (recall that the polyhedron for  $n = 12$  is the icosahedron) then the minimizing configuration tends to have rather low symmetry.

For  $n \geq 12$  most of the polyhedra consist of  $2(n-2)$  triangular faces with 12 pentamers and  $n-12$  hexamers. Particularly symmetric examples are the icosahedron at  $n=12$  and the dual of the truncated icosahedron at  $n=32$ . Within the range we have studied,  $12 \leq n \leq 32$ , there are six exceptions to the above rule, at  $n=13, 18, 19, 21, 24, 25$ . As can be seen from figs. 3,4, the polyhedra for  $n=13, 18, 21$  contain tetravalent vertices (one each for  $n=13, 21$  and two in the case of  $n=18$ ) and for  $n=19, 21, 24, 25$  there are rectangular faces (one each for  $n=19, 21, 25$  and six squares for  $n=24$ , which is a slightly deformed snub cube).

The Platonic solids with trivalent vertices (the cube at  $n=8$  and the dodecahedron at  $n=20$ ) are clearly not favoured by the desire for triangular faces and the formation of pentamers and hexamers, so it is not surprising that these highly symmetric configurations do not arise.

Polyhedra (or their duals) with  $n$  vertices and  $2(n-2)$  triangular faces forming 12 pentamers and  $n-12$  hexamers appear to be generic configurations of points which arise in a number of diverse applications. Examples include carbon chemistry, where the dual polyhedra appear with vertices representing the positions of the carbon atoms in closed cages known as fullerenes [8], in biology, where they arise in the structure of spherical virus shells [4], and in Skyrmions, which are topological solitons which model nuclei. In this last application the vertices of the dual polyhedra represent points at which the baryon density is maximal. The relation between the number of points  $n$  and the baryon number  $B$  is  $n=2B-2$ . Comparing the results in this paper with those in [3] we find that for  $2 \leq B \leq 22$ , which is the range of baryon numbers for which Skyrmion results are known, there is an exact match between the symmetries and combinatorial types of the Skyrmion polyhedra and the duals of the polyhedra presented here, for all but five cases ( $B=5, 9, 10, 19, 22$ ), and in some of these cases there is a match with known low energy local minima Skyrmions, whose energies are extremely close to those of the global minima.

Rather surprisingly, it appears that the arrangement of point charges on a sphere is closely related to the configurations of points we have generated by our purely geometrical construction. The details of this comparison are addressed in the following section.

## 6 Comparison with charges on a sphere

The problem, generally attributed to J.J. Thomson [11], is to find the configuration of  $n$  point charges on the surface of a sphere such that the total Coulombic energy

$$E_1 = \sum_{i>j}^n \frac{1}{|\mathbf{x}_i - \mathbf{x}_j|} \quad (6.1)$$

is minimal. This is a notoriously difficult problem, but the use of modern computers has provided numerical results for  $2 \leq n \leq 112$ , see for example [7] and references therein. Remarkably we find that for all  $2 \leq n \leq 32$  the symmetries of the configurations we have found are identical to those of the configurations of points on a sphere which minimize the energy (6.1) (compare table 1 with table 1 of [6]). Furthermore, the combinatorial types of

the polyhedra also match. Note that it is not true that all the configurations are identical in each case, since our points are not constrained to lie on the surface of a sphere, and in some cases it appears that they definitely do not. However, as we have seen, in all cases the points lie very close to the surface of a sphere and so it is possible to consider projecting them onto the sphere. Since there is always an ambiguity in performing such a projection we have instead adopted an approach which is mathematically better defined, namely, we constrain the points to lie on the surface of the unit sphere throughout the minimization process. Practically the two approaches agree, since the resulting minimal energy configurations are identical to those obtained by projection of the previous configurations, to within the accuracy that we work (associated with the values listed in table 1).

These configurations of points on a sphere agree with those that minimize the Coulomb energy, to within the accuracy that we work. For example, we have taken each of our minimal energy configurations and computed their Coulomb energies (6.1) and compared these with the table presented in [7], where we find an agreement to at least five significant figures in each case. Also, comparing figs. 3 and 4 with the corresponding figures in [6] it can be verified that the combinatorial types are identical. This correspondence is intriguing, given our purely geometric construction, which is scale invariant and certainly has no explicit 2-particle interaction, but yet appears to generate an interaction which confines the particles close to a sphere and has the same affect as the Coulomb force. It is true that for a small number of points  $n \leq 6$ , the minimal arrangement is essentially independent of the force law and is determined by symmetry alone, but for  $n \geq 7$  the precise arrangement and symmetry of the minimizing configuration is sensitive to the energy formula used. For example, if the Coulomb interaction (6.1) is replaced by a more general power law

$$E_p = \sum_{i>j}^n \frac{1}{|\mathbf{x}_i - \mathbf{x}_j|^p} \quad (6.2)$$

then the symmetry and structure of the minimal energy configuration can be studied as a function of  $p$  (and  $n$ ) with highly non-trivial results [9]. We shall return to this point later in Section 9. As an illustration, the Tammes problem (to determine the configuration of  $n$  points on a sphere so that the minimum distance between the points is maximized) emerges from the potential (6.2) in the limit  $p \rightarrow \infty$  and numerical results show that for  $n > 6$  the only configuration which is a common solution of the Coulomb and Tammes problem is the icosahedral arrangement for  $n = 12$  [7]. This makes our observed matching with the Coulomb problem even more remarkable and it would be interesting to see if this pattern continues for larger values of  $n$ .

In the Coulomb problem there are a number of local minima with energies which are only very slightly above that of the global minimum, but have completely different symmetries. In fact the number of stable local minima appears to grow exponentially fast with  $n$  [7]. The smallest number of points for which such a metastable state occurs in the Coulomb problem is  $n = 16$  and this is again mirrored in our findings, with a local minimum produced at  $n = 16$  with  $D_{4d}$  symmetry and an energy of  $E = -24.9477$ , in comparison with the  $T$  symmetric global minimum with energy  $E = -24.9525$ . The existence of metastable states

is one of the motivations for our use of a simulated annealing algorithm combined with a number of different random starting configurations.

## 7 Comparison with a 3-particle interaction

As we saw in the previous section, if the points are constrained to lie on the surface of a sphere then a good approximation to the configurations which minimize our multi-particle energy are obtained by minimizing the 2-particle Coulomb energy. The question we address in this section is whether there exists a 2-particle or 3-particle energy which provides the same kind of good approximation, in the sense of generating almost the same minimizing configurations, but which has the additional features of being scale invariant (in common with our multi-particle energy) and does not require the points to be constrained to the surface of a sphere.

Clearly, there can be no scale invariant 2-particle energy, which preserves rotational invariance, since the only possible quantity from which to form an interaction is the distance between the two points. We therefore turn our attention to a possible approximation involving a 3-particle interaction.

In view of conjecture 3 applied inductively we can express our  $n$ -particle energy function  $E$  as a sum of ‘pure’  $k$ -particle energies  $F_k$ , for  $k = n, n-1, \dots, 3$ . For example, the conjectured inequality (5.3), leads us to define  $F_n$  as

$$F_n = E - \frac{1}{n-2} \sum E_i \quad (7.1)$$

(and so  $F_n \leq 0$ ). Next we would define

$$F_{n-1} = \frac{1}{n-2} \sum E_i - \frac{2}{(n-2)(n-3)} \sum E_{ij} \quad (7.2)$$

(where the second sum is over pairs  $i > j$ ) with  $F_{n-1} \leq 0$ . Continuing in this way we can express

$$E = F_n + F_{n-1} + \dots + F_3 \quad (7.3)$$

as a sum of (conjecturally) negative terms : the parts of the energy which are not consequences of energies of proper subsets.

In usual physical models a complicated multi-particle energy function can sometimes be expanded as a sum of pure  $k$ -point energies, starting with  $k = 2$ , and this 2-point energy may be the dominant factor. Here our expansion (7.3) starts with  $k = 3$ , but by analogy we might conjecture that this is in some sense the ‘dominant part’. Thus we are led, very tentatively, to compare our energy function  $E$  with the 3-point energy function  $F_3$ . In particular we will compare the minimal configurations of these two energy functions. We will find remarkable agreement which will be quantified.

Although we have the (conjectured) inequality

$$E \leq F_3 \quad (7.4)$$

it will, for some purposes, be more enlightening to rescale  $F_3$  by a numerical constant. The reason is that

$$F_3 = \frac{1}{n-2} \sum E_I \quad (7.5)$$

where  $I$  runs over all (unordered) triples in  $(1, 2, \dots, n)$  and  $E_I$  is the energy of the corresponding triangle of points in  $\mathbb{R}^3$ . But the number of such triangles (or triples) is just

$$\binom{n}{3} = \frac{n(n-1)(n-2)}{6} \quad (7.6)$$

and so the *average energy per triangle* is

$$E_\Delta = \frac{6}{n(n-1)(n-2)} \sum E_I = \frac{6}{n(n-1)} F_3. \quad (7.7)$$

Note that, as an approximation to  $E$ ,  $E_\Delta$  is very much worse than  $F_3$ . On the other hand it is a natural quantity to measure numerically and in particular it will have a sensible asymptotic behaviour for large  $n$ , as we shall postulate. Explicitly,  $E_\Delta$  is given by the formula

$$E_\Delta = \frac{-6}{n(n-1)(n-2)} \sum_{i>j>k} \log \left\{ \frac{1}{2} \left[ \sin^2 \left( \frac{\theta_1 + \theta_2}{2} \right) + \sin^2 \left( \frac{\theta_2 + \theta_3}{2} \right) + \sin^2 \left( \frac{\theta_3 + \theta_1}{2} \right) \right] \right\} \quad (7.8)$$

where  $\theta_1, \theta_2, \theta_3$  are the angles in the triangle formed by the three points  $\mathbf{x}_i, \mathbf{x}_j, \mathbf{x}_k$ , and we have used the explicit formula (3.16) for the 3-particle volume.

In fig. 5 we plot (crosses) the minimal value of  $E_\Delta$  for  $n$  points with  $3 \leq n \leq 32$ . The precise values are presented in the fifth column of table 1. Again these results are obtained using a multi-start simulated annealing code. For  $n = 3$  and  $n = 4$  the minimal value of  $E_\Delta$  is obviously  $-\log(9/8)$ , since in these two cases all triples of points can simultaneously be made to form equilateral triangles; this being achieved by the regular tetrahedron in the case of four points. For  $n > 4$  the energy rises, though rather slowly, and already at 32 points it has clearly begun to level off. It seems probable that an upper bound for the energy  $E_\Delta$  is obtained by the average value of the 3-particle energy for three randomly distributed points. By numerically computing the values for 50,000 randomly chosen triangles we find that this average value is  $\bar{E}_\Delta = -0.078$ . The constant  $\bar{E}_\Delta$  is indicated in fig. 5 as a dashed line, and is consistent with the numerical results. Further simulations, for larger values of  $n$  are required to determine whether the minimal value of  $E_\Delta$  asymptotes to the value  $\bar{E}_\Delta$ , given by randomly distributed points, or whether it tends to a slightly lower level.

The aim of this section was to find an energy which was a sum of 3-particle interactions such that the arrangement of minimizing points closely reproduces the earlier results based on the multi-particle energy  $E$ . The energy  $E_\Delta$  succeeds in this aim, with the positions of all points of the  $E_\Delta$  minimizing configurations being within 1% of those in the  $E$  minimizing arrangements. A more quantitative comparison is made in table 1 where we list the quantity  $\tilde{E}$ , which is the value calculated for the energy  $E$  from the  $E_\Delta$  minimizing configuration. A comparison between  $E$  and  $\tilde{E}$  demonstrates the close match between the two sets of

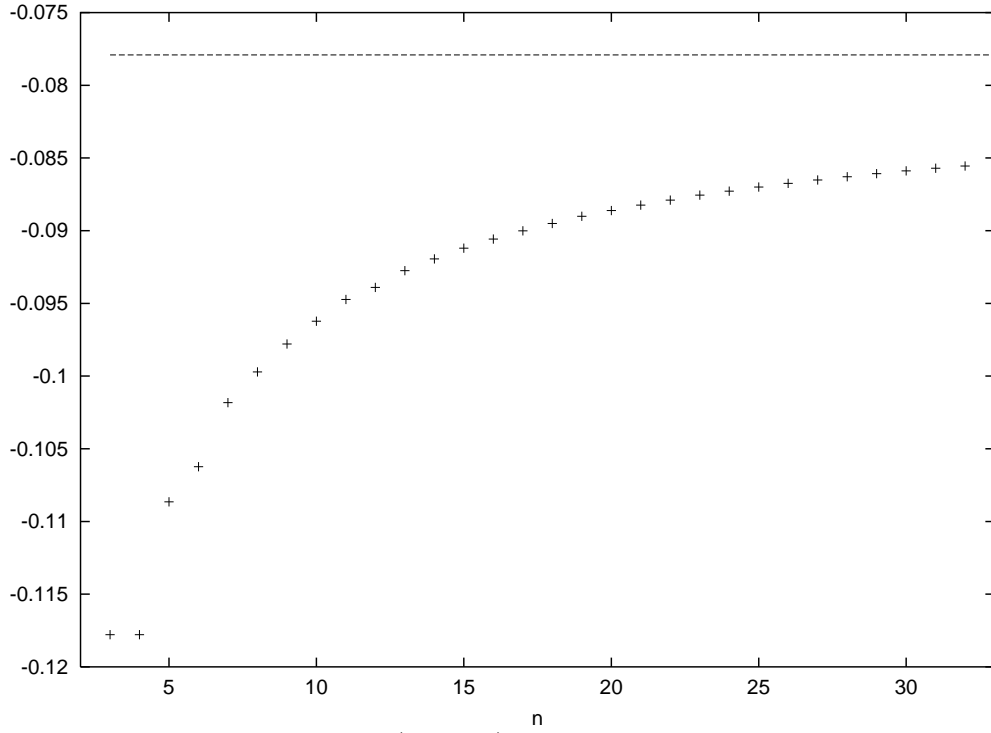


Figure 5: The minimal value (crosses) of the energy  $E_\Delta$  for  $n$  points in the range  $3 \leq n \leq 32$ . The dashed line represents the average value of  $E_\Delta$  for three randomly distributed points.

configurations and confirms that  $E_\Delta$  is a good approximation. The worst match is for  $n = 5$ , where the three points which form an equilateral triangle lie on a circle whose radius is increased by less than  $\frac{1}{2}\%$  in comparison with the  $E$  minimizing configuration, though otherwise these two configurations are identical. In the last column of table 1 we list, for comparison with  $\delta$ , the deformation from a spherical arrangement,  $\tilde{\delta}$ , (computed in the same way as  $\delta$ ) for the  $E_\Delta$  minimizing points.

The energy function  $E_\Delta$  helps us to understand why the configurations we produce are spherical polyhedra with faces which are generally triangular. This is because, locally, the arrangement of points favours equilateral triangles, and if we consider introducing an additional point, far from a current spherical distribution, then clearly all the triangles involving this point will have one very acute angle, which can be increased by moving the point closer to the shell, hence lowering the energy and producing an attraction.

## 8 The unconstrained problem

In Section 3 we defined a complex-valued function  $D$  on the open set  $t_{ij} \neq t_{ji}$  in a product of  $n(n - 1)$  2-spheres. We then restricted it to half the number of 2-spheres by taking  $t_{ji}$

to be the anti-pode of  $t_{ij}$ . The energy function  $E$  on  $\mathcal{C}_n(\mathbb{R}^3)$  which we have been studying was defined by

$$E = -\log |D| \quad (8.1)$$

evaluated on the  $t_{ij}$  defined by  $(\mathbf{x}_1, \dots, \mathbf{x}_n)$  as in (2.2). We have the conjectured inequality  $E \leq 0$  and we have, in previous sections, been investigating the configurations  $(\mathbf{x}_1, \dots, \mathbf{x}_n)$  which minimize  $E$ . We now ask how do these compare with the configurations of  $t_{ij}$  which minimize  $E$ , without the constraint required by (2.2), that the  $t_{ij}$  originate from a configuration of points in  $\mathbb{R}^3$ . Note that the space of  $t_{ij}$  has real dimension  $n(n-1)$ , while  $\mathcal{C}_n(\mathbb{R}^3)$  has dimension  $3n$  (and reduces to  $3n-4$  when we factor out by translation and scale, which do not affect  $E$ ). Thus there are many constraints. For  $n=3$  we have

$$n(n-1) = 6, \quad 3n-4 = 5 \quad (8.2)$$

so that there is one constraint. It is that the 3 points  $t_{12}, t_{13}, t_{23}$  lie on a great circle (and also form an acute-angled triangle). It therefore seems to be quite remarkable, and presumably significant, that a numerical investigation suggests that the minimum energy of the constrained and unconstrained problems coincide, as do the corresponding configurations. This may well be a clue to explaining why our energy minimizing configurations have such striking properties.

Although the constrained and unconstrained problems appear to have the same minima for the energy, the corresponding statement for the maxima is definitely false. In fact, for the unconstrained problem the energy can be infinite or equivalently the function  $D$  can vanish. This happens already for  $n=3$  with  $t_{12} = t_{23} = \infty$  and  $t_{13} = 0$ , so that the 3 polynomials  $p_i$  all coincide (having 0,  $\infty$  as the 2 roots) and hence are linearly dependent.

One might be tempted to combine the unconstrained problem of this section with the 3-point energy of the previous section, and determine the unconstrained configurations of  $t_{ij}$  which minimize the average energy per triangle  $E_\Delta$ , summed over all triples of  $t_{ij}$  with  $i < j$ . However, a numerical study reveals that for  $n > 3$  the minimal configurations for this problem do not resemble our earlier configurations.

## 9 The planar restriction

It is interesting to investigate the minimal energy configurations for points in the plane, that is, we restrict our configuration space to  $(\mathbf{x}_1, \dots, \mathbf{x}_n) \in \mathcal{C}_n(\mathbb{R}^2)$ . Again we can make use of the translation and scale invariance of our problem to fix the centre of mass at the origin and make all the points lie in the unit disc  $|\mathbf{x}_i| \leq 1$ , with at least one point on the boundary.

The results for  $2 \leq n \leq 15$  are perhaps not surprising, with the  $n$  points lying on the unit circle and forming the vertices of a regular  $n$ -gon. However, for  $n=16$  the minimal energy configuration consists of a regular 15-gon on the unit circle and a single point at the origin. These points are displayed in fig. 6.16.

The pattern of an  $(n - 1)$ -gon plus one point at the centre continues until  $n = 23$ , at which point the configuration comprises a 21-gon plus two points placed in the interior of the disc equidistant from the origin and lying on a diameter. This is displayed in fig. 6.23.

At  $n = 28$  a further point enters the interior of the disc, producing a 25-gon with an equilateral triangle inside; fig. 6.28. At  $n = 33$  another point enters the interior of the disc, leading to a 29-gon with a square arrangement at the interior; fig. 6.33. Note that the points in the interior are always arranged in the minimal energy configuration of that number.

We refer to the sequence of numbers,  $n = 16, 23, 28, 33, \dots$  at which an additional point enters the interior of the disc, as the jumping values.

In addition to the global minimum energy configurations described above we have found a large number of local minima, associated with one or more points moving from the interior of the disc to the boundary, or vice-versa. A large number of annealing runs were made in each case to find all the local minima and hence determine the global ones.

Our energy function is scale invariant, so it is interesting that for  $n > 22$  a scale has emerged, given by the ratio of the radius of the interior circle to that of the bounding disc. Presumably these radii, which increase slightly with  $n$ , have some universal geometrical character.

It is useful to repeat our earlier comparisons with 2-particle and 3-particle interactions, applied to the planar case.

First, we consider the Coulomb interaction. If  $n$  point-particles in the unit 3-ball interact via the 2-particle Coulomb energy (6.1) then the minimal energy configurations consists of points which all lie on the unit sphere. The relevant theorem here is that a harmonic function on a bounded domain takes its minimal value on the boundary of the domain. However, if we consider the planar version, so that the points are confined to the unit disc, then the configuration of points which minimizes the Coulomb energy (6.1) can include points which lie in the interior of the disc. This is because the Coulomb energy is a harmonic function in three-dimensions but not in two-dimensions. If the Coulomb energy is replaced by a logarithmic energy then this is harmonic in two-dimensions and so all points lie on the unit circle for the global minimizer.

The configurations which are the global minima for the Coulomb energy of points in a disk have been computed numerically for up to 80 points in [10]. A glance at the figures in this reference show an immediate qualitative similarity with those in fig. 6. For  $n < 12$  the points form a regular  $n$ -gon on the unit circle. For  $12 \leq n \leq 16$  they form an  $(n - 1)$ -gon with a single point at the centre of the disc. For  $n = 17, 18$  there are two points in the interior of the disc which lie on a diameter, in the same manner as in fig. 6.23. For  $n = 19, 20, 21$  there are three interior points which form an equilateral triangle, as in fig. 6.28. For  $n = 22, 23, 24$  there are four interior points on the vertices of a square, which is the arrangement in fig. 6.33. Thus it seems that the same patterns emerge in the Coulomb case as for our energy minimizers, though the jumping values, at which additional points enter the interior of the disc, are shifted to the sequence  $n = 12, 17, 19, 22, \dots$  Thus the jumps occur earlier and more frequently for the Coulomb energy. For larger values of  $n$  the number of shells (circles on which  $m$  points approximately lie on a regular  $m$ -

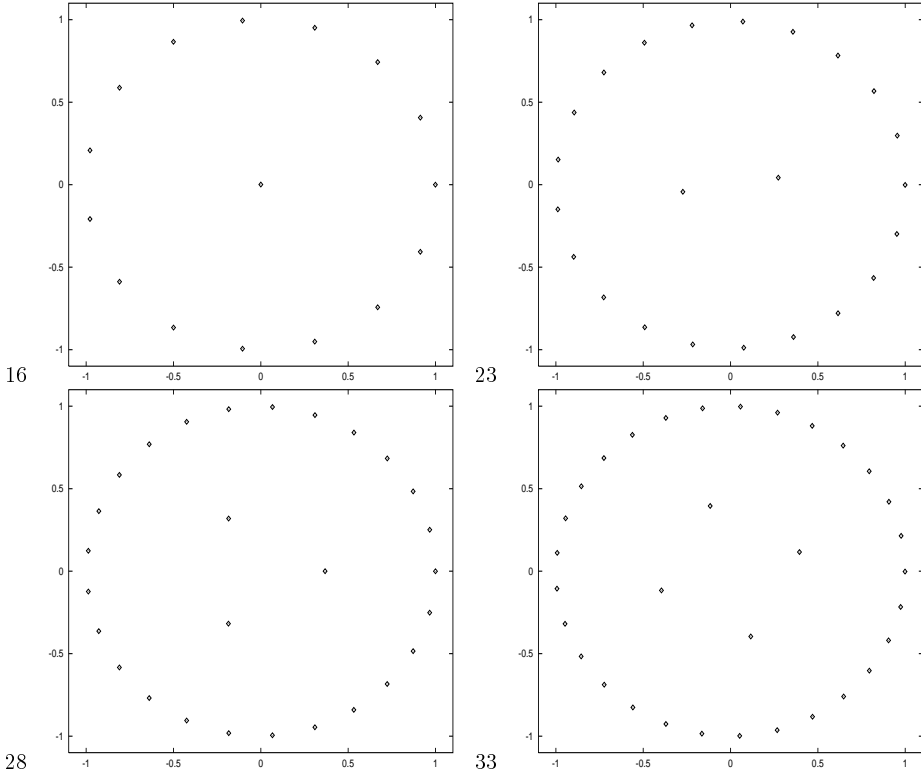


Figure 6: The positions of the energy minimizing points in the plane for the jumping values  $n = 16, 23, 28, 33$ .

gon) increases beyond two, so that, for example, at  $n = 80$  there are four shells containing 4, 10, 18, 48 points respectively, working from the inner shell out to the boundary of the disc. We therefore expect that for larger  $n$  a similar pattern of increasing shells will emerge as the minimizers of our geometric energy, though the number of points required to generate a given number of shells will be larger than for the Coulomb energy.

The above results suggest that the planar case is more sensitive to the form of the energy function than the three-dimensional problem, since in three-dimensions we found a much closer agreement between the minimizers of our energy and those of the Coulomb energy. This may be due to the fact that points interacting via a Coulomb energy automatically lie on the surface of a sphere, so there is no issue of matching the number of interior points. This explanation appears likely, given that the arrangements of interior and boundary points also agrees for the two energies in the planar case, it being the *number* of interior points which fails to match.

We can make use of the sensitive nature of the planar restriction to investigate whether

there is a power  $p$ , in the more general 2-particle energy (6.2) for which a better approximation to our multi-particle energy configurations can be achieved than the Coulomb case of  $p = 1$ . This indeed turns out to be the case. First of all, requiring the first jumping value to be at  $n = 16$  determines that  $p$  lies in the small range  $0.58 < p < 0.64$ . If  $p$  lies outside this range then the jump to a single point in the centre of the disc occurs at a smaller or larger value of  $n$  than 16. Although the second jumping value,  $n = 23$ , can also be matched, we find that there is no value of  $p$  within this range such that the third jumping value occurs at  $n = 28$ . Thus, there is no value of  $p$  such that the energy minimizing configurations agree for all  $n$ , but choosing  $p = 0.6$  gives a good approximation, with the jumping values being  $n = 16, 23, 27, 31, \dots$ . The arrangements of points for values of  $n$  which have the same number of interior points are essentially identical.

An obvious question is to ask about the minimal arrangements of points on a sphere interacting with the energy (6.2) for the selected value of  $p = 0.6$ . Computing these configurations we find that they agree with those of the Coulomb energy,  $p = 1$ , to within the accuracy that we made the earlier comparison with our energy function. Given our earlier comments, then for much larger values of  $n$  it might be expected that a noticeable difference may emerge between the case  $p = 0.6$  and  $p = 1$ . As far as we are aware the minimal energy configurations for the more general energy (6.2) have been studied only for  $p \geq 1$ .

If we compare with the three-particle energy,  $E_\Delta$  given by (7.8), restricted to the planar case we again find the same patterns of points, but the precise jumping values are even further away from those of the multi-particle energy than for the Coulomb approximation. Explicitly, the jumping values are  $n = 8, 12, 14, 16, \dots$ .

## 10 Points in hyperbolic space

If we replace Euclidean space  $\mathbb{R}^3$  by hyperbolic 3-space, which we denote by  $\mathbb{H}_\kappa^3$ , where  $-\kappa^2$  is the curvature, then there is an analogue of the Berry-Robbins problem, together with all the other issues we have addressed in the Euclidean case, such as the configurations of points which minimize a geometrical multi-particle energy. This was already noted in [1, 2].

The natural generalization to hyperbolic space is to ask for a map

$$F_n : \mathcal{C}_n(\mathbb{H}_\kappa^3) \mapsto GL(n, \mathbb{C}) / (\mathbb{C}^*)^n. \quad (10.1)$$

which is compatible with the action of  $\Sigma_n$  and  $SL(2, \mathbb{C})$ , where this acts (modulo  $\pm 1$ ) on hyperbolic space as its group of (oriented) isometries and on  $GL(n, \mathbb{C})$  via the irreducible  $n$ -dimensional representation.

The construction of Section 2, based on the polynomials  $p_1, \dots, p_n$  can be repeated in hyperbolic space in a similar way. Given two distinct points  $\mathbf{x}_i, \mathbf{x}_j \in \mathbb{H}_\kappa^3$ , we define  $t_{ij}$  to be the point on the Riemann sphere at infinity along the oriented geodesic through  $\mathbf{x}_i$  and  $\mathbf{x}_j$ . Note that in the hyperbolic case  $t_{ij}$  and  $t_{ji}$  are no longer antipodal points on the Riemann

sphere: in fact the notion of anti-pode requires us to fix an origin in  $\mathbb{H}_\kappa^3$ , and is not  $SL(2, \mathbb{C})$  invariant.

We take the projective model of  $\mathbb{H}_\kappa^3$ , as the interior of the 3-ball of radius  $1/\kappa$  in  $\mathbb{R}^3$ . The geodesics are then just straight lines, and  $t_{ij}$  is the point where the (oriented) line  $\mathbf{x}_i \mathbf{x}_j$  meets the sphere of radius  $1/\kappa$  in  $\mathbb{R}^3$ . In the zero curvature limit,  $\kappa \rightarrow 0$ , of the hyperbolic construction, we recover the earlier Euclidean case.

A geometric proof of the independence of the polynomials  $p_1, \dots, p_n$  can be given for  $n = 3$  [1], but the hyperbolic version of conjecture 1 still remains unproven for  $n > 3$ .

The complex function  $D$  of the  $t_{ij}$  introduced in Section 3 is still well-defined because we always have  $t_{ij} \neq t_{ji}$ . It is covariant under the full isometry group of hyperbolic space with reflections inducing complex conjugation. Assuming  $D \neq 0$  (the hyperbolic conjecture) we can again define a volume  $V = |D|$  and an energy function

$$E = -\log V. \quad (10.2)$$

This definition is  $SL(2, \mathbb{C})$  invariant and so is intrinsic to hyperbolic space.

The numerical evidence again supports the hyperbolic version of conjecture 2, namely  $V \geq 1$  or  $E \leq 0$ .

Turning now to the minimizers of the energy  $E = -\log V$ , we find that the same arrangements of points as in Euclidean space are the minimizers, but there is now an intrinsic scale, provided by the curvature of hyperbolic space, and the energy is minimized in a singular limit as the overall scale of the configuration tends to zero. In other words the curvature of hyperbolic space provides an attractive force. This can be illustrated by considering the simple case of an equilateral triangle with a varying scale.

Consider the equilateral triangle with vertices on the circle centered at the origin and of radius  $\rho/\kappa$ , where  $0 < \rho < 1$ . An explicit calculation of the energy for this configuration yields

$$E = -\log \left\{ \frac{3\sqrt{3}(\sqrt{12 - 3\rho^2} - \rho)}{2(4 - \rho^2)^{3/2}} \right\}. \quad (10.3)$$

This energy, as a function of  $\rho$ , is displayed in fig. 7 as the dashed curve. The minimum is attained in the singular limit  $\rho \rightarrow 0$ , where the Euclidean result  $E = -\log(9/8)$  is recovered. The scale invariance of the Euclidean case emerges by taking the limit  $\kappa \rightarrow 0$  and  $\rho \rightarrow 0$  such that the ratio  $\rho/\kappa$  is finite, and gives the arbitrary scale of the triangle.

It may be possible, by the addition of an extra repulsive contribution to the energy, to balance the attraction induced by hyperbolic space, but, as yet, we have not found an elegant way to incorporate such a modification.

An alternative to the addition of extra terms is to exploit the attraction of hyperbolic space to construct bound orbits of rotating configurations. As an example, let us reconsider the above configuration of three points on an equilateral triangle with scale  $\rho/\kappa$ . Keeping the plane of the triangle fixed, introduce an angle  $\phi$  describing the freedom to rotate the triangle about its centre. 3-particle configurations have a fixed point set under the dihedral group  $D_{3h}$  which is two-dimensional, and is parametrized by the coordinates  $\rho$  and  $\phi$  which we have introduced. When discussing time dependent solutions it is therefore a consistent

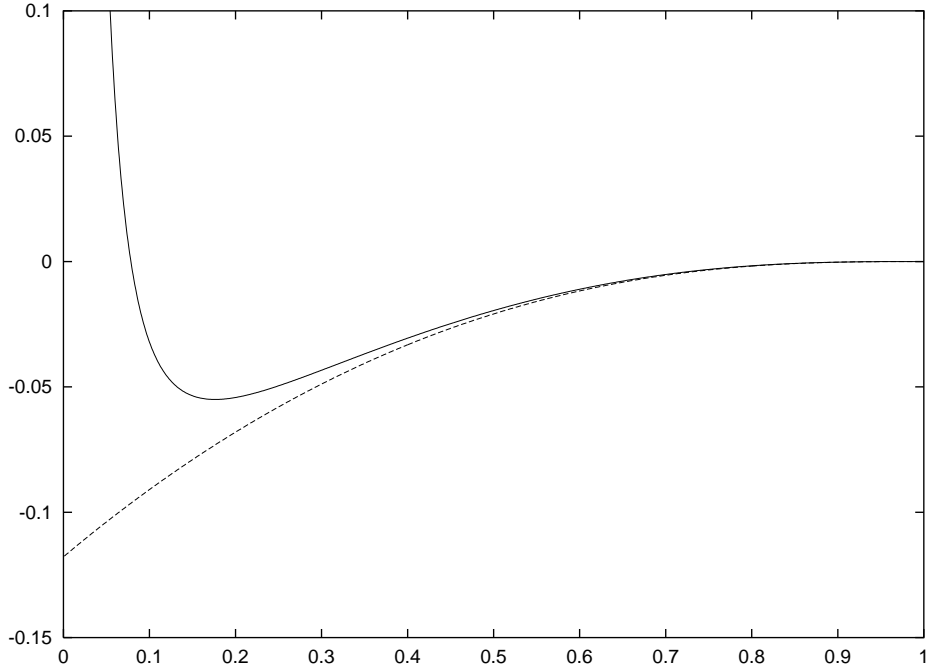


Figure 7: Two quantities (as a function of  $\rho$ ) associated with three points on the vertices of an equilateral triangle of scale  $\rho/\kappa$  in hyperbolic space. The dashed curve is the energy  $E$  of the static configuration. The solid curve is the total energy  $U$  for a rotating triangle with angular momentum  $l = 0.02$ .

reduction to restrict to the two-dimensional dynamical system given by  $\rho(t), \phi(t)$ . Taking the point particles to have unit mass, the Lagrangian for this system is given by

$$\mathcal{L} = \frac{3}{2\kappa^2(1-\rho^2)^2}(\dot{\rho}^2 + \rho^2\dot{\phi}^2) - E \quad (10.4)$$

where  $E$  is the potential energy given by (10.3) and dot denotes differentiation with respect to the time coordinate  $t$ .

The expression for the conserved angular momentum is

$$l = \frac{\rho^2\dot{\phi}}{(1-\rho^2)^2}. \quad (10.5)$$

For a solution to exist that describes a triangle with fixed radius which rotates at constant angular velocity  $\dot{\phi}$  therefore requires a solution of the equation

$$\frac{dU}{d\rho} = 0, \quad \text{where} \quad U(\rho) = E + \frac{3l^2}{2\kappa^2} \frac{(1-\rho^2)^2}{\rho^2}. \quad (10.6)$$

Providing the angular momentum  $l$  is not too large, then solutions of this equation indeed exist with  $\rho \in (0, 1)$ . For example, for  $\kappa = 1$  and  $l = 0.02$  the total energy  $U(\rho)$  is plotted (solid curve) as a function of  $\rho$  in fig. 7. This function has a clear minimum (which occurs at  $\rho = 0.176$ ) demonstrating the existence of a dynamical solution describing three orbiting points on the vertices of an equilateral triangle associated with this finite non-zero scale. The fact that this critical point is the global minimum also shows that this orbit is stable within the class of rotating triangular solutions. Similarly, one expects more complicated orbiting configurations to exist for larger numbers of particles.

In Euclidean space reflection in an origin interchanges  $t_{ij}$  and  $t_{ji}$ , since these are anti-podes, and the function  $D$  gets conjugated by such a reflection. Thus interchanging the roles of the two indices in  $t_{ij}$  takes  $D$  into  $\bar{D}$ . This is not a trivial observation since we get the  $p_i$  by symmetrizing over  $j$  and then (taking the exterior product) we skew-symmetrize over  $i$ . In hyperbolic space, where we have no usual notion of anti-pode, we cannot argue in this way. In fact reversing the roles of the indices in  $t_{ij}$  produces a quite *different function*  $D^\dagger$ .

As noted at the end of [2] hyperbolic geometry is closely related to Minkowski geometry because of the isomorphism (of connected groups)

$$SL(2, \mathbb{C}) \cong \text{Spin}(3, 1). \quad (10.7)$$

In [2] it was shown how to attach points  $t_{ij}$  to  $n$  points (or events) in Minkowski space *with their past histories* (or world-lines). Although not entirely obvious it is true (and was observed in [2]) that  $t_{ij} \neq t_{ji}$ . Hence, proceeding as in Section 3, we can still define our complex-valued function  $D$  (which may now have zeros). It has full Lorentz-invariance because of (10.7), but we have to be careful about the disconnected components corresponding to space reflection and time-reversal. As before, space-reflection takes  $D$  into  $\bar{D}$ , but time-reversal is, in general, not allowable since it would take past histories into the (unknown) future. However, we can apply it in the very special case of particles travelling along straight-lines (ie. uniform motion) and all emerging from a ‘big-bang’ in the past. As shown in [2] this essentially reduces to pure hyperbolic geometry and time-reversal in this case makes sense (with a forecast future of continuing uniform motion) and takes  $D$  into the different function  $D^\dagger$ . In fact this holds provided each pair of world-lines are (and remain) coplanar - the motion need not be uniform.

This complex function  $D$ , depending on past histories, raises interesting physical questions and its implications will be considered more carefully on a future occasion. It has been suggested to us by Michael Berry that it may be related to the use of retarded potentials in the relativistic treatment of the dynamics of charged particles.

## 11 The complex phase

So far in this paper we have made extensive use of the real volume,  $V = |D|$ , but we have ignored the phase of the complex function  $D$ , associated with the volume form.

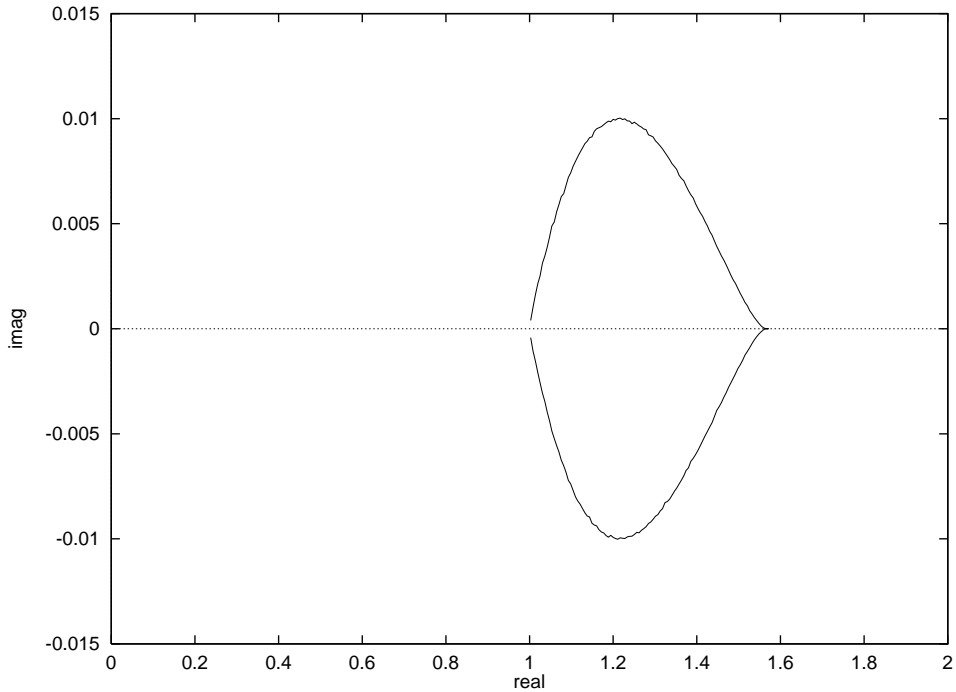


Figure 8: The curves bounding the region of the complex plane where  $D$  takes its values for  $n = 4$ .

As explained in Section 3, if a configuration of  $n$  points in  $\mathbb{R}^3$  has a reflection symmetry then  $D$  is automatically real, and so  $D$  is always real for  $n < 4$ . It is to be expected that for a general arrangement of four or more points then  $D$  will be complex, but the region of the complex plane where  $D$  takes its values is by no means obvious. In this brief section we investigate this aspect for the simplest case of four points. By computing  $10^7$  random configurations of four points we have been able to map out the region of the complex plane in which  $D$  is constrained to lie for  $n = 4$ . It is the interior of the region bounded by the solid curves in fig. 8. Note the differing scales on the real and imaginary axes, indicating that the complex part of  $D$  is very small for all configurations of four points; in fact the phase angle is always less than one degree, which is quite surprising. An obvious question concerns the configuration of points for which the phase angle is maximal, and this has an amusing answer. Recall that the phase is zero if there is a reflection symmetry, so in some sense this configuration should be maximally asymmetric, but in a controlled rather than random way. This is precisely what happens, with the four points arranged in two groups of two and lying in two parallel planes. The angle between the lines joining each of the coplanar points is  $45^\circ$  and it is in this sense that the asymmetry is maximal, since if this angle is zero then all four points are coplanar and hence the phase is zero. Similarly if this angle is  $90^\circ$  then again there is a reflection symmetry, this time the reflection plane contains two of the coplanar points and the reflection leaves these two points fixed and

exchanges the remaining two. Thus the observed  $45^\circ$  angle is precisely mid-way between two possible values of the angle for which there is a reflection symmetry.

We have performed similar calculations for more points and the results are qualitatively similar, with the allowed region of the complex plane having a shape of the same form as for  $n = 4$ , but being of slightly larger area. Consequently the maximal value of the phase grows slightly with  $n$ , and more complicated maximally asymmetric configurations occur.

## 12 Conclusions

This paper began with the aim of numerically verifying conjecture 1, establishing the existence of a certain natural map  $\mathcal{C}_n(\mathbb{R}^3) \mapsto U(n)/U(1)^n$ . For this purpose we introduced a complex function  $D$  on the configuration space  $\mathcal{C}_n(\mathbb{R}^3)$  and the associated ‘energy’ function  $E = -\log|D|$ . Numerical simulations applied to  $|D|$  not only verified (for  $n \leq 20$ ) the inequality  $|D| > 0$  (implying conjecture 1), but also suggested the stronger inequality  $|D| \geq 1$ , with equality only for collinear configurations. This encouraged us to make our second conjecture, which in terms of the energy asserts that  $E \leq 0$ .

Calculations for  $n = 3$  then suggest a more precise inductive inequality

$$E \leq \frac{1}{n-2} \sum E_i \quad (12.1)$$

where  $E_i$  is the energy of the configuration of  $n-1$  points obtained by omitting  $\mathbf{x}_i$ . Numerical calculations substantiated this and so encouraged us to make (12.1) our third conjecture.

We were then led, out of pure curiosity, to ask the opposite question about the minimum value of  $E$  and the configurations which produce this minimum. Very surprisingly, we found them (up to  $n = 32$ ) to be approximately spherical polyhedral structures of high symmetry. It appears that these particular polyhedra (or their duals), comprising  $n$  vertices and  $2(n-2)$  triangular faces forming 12 pentamers and  $n-12$  hexamers, are somewhat generic configurations. They arise in a number of complicated 3-dimensional physical applications (eg. Skyrmions, fullerenes), as well as in the 2-dimensional problem for configurations of Coulomb charges on a sphere.

Given the basic geometric nature of our problem, with its energy function, it may well be that it is the simplest example of a whole universality class of similar effective interactions. It may therefore be a useful model and can perhaps act as a simple approximation to more complicated physical systems. For example it should be possible to use our minimum energy configurations as a basis for predicting the structure of higher charge Skyrmions and even of constructing them.

In an attempt to understand why our energy function leads to these kind of minima we were led to look at two simplifications of the problem. In the first we replaced our energy function by its associated 3-point energy, by taking the energy function for  $n = 3$  (given by a simple explicit formula) and summing it over all triples in our set of  $n$  points. We found (numerically) essentially the same minimum energy configurations, indicating that this 3-point energy is in some sense the dominating part of the total energy.

The second simplification we made was to compute the energy function for all sets of points  $t_{ij}$  on the 2-sphere (with  $t_{ji}$  the anti-pode of  $t_{ij}$ ), without requiring the constraint that they arise as the set of directions joining points  $\mathbf{x}_i, \mathbf{x}_j$  of a configuration in  $\mathcal{C}_n(\mathbb{R}^3)$ . We refer to this as the unconstrained energy problem and again (numerically) we found the same set of minima.

All these results seem to indicate some underlying and very stable phenomenon, and following up on the various simplifications may yield a better theoretical understanding of what is, at present, computer evidence. There are a number of very interesting mathematical results concerning the space of shapes of polyhedra and triangulations of the sphere [12] and these may prove useful in further theoretical investigations.

Finally we investigated two variants of our energy problem. One is to restrict to planar configurations, and the other is to replace Euclidean space by hyperbolic space. The latter may have interesting consequences in Minkowski space.

## Acknowledgements

Many thanks to Richard Battye for useful discussions.

PMS acknowledges the EPSRC for an advanced fellowship.

## References

- [1] M.F. Atiyah, *The Geometry of Classical Particles*, Surveys in Differential Geometry (International Press) 7, 1 (2001).
- [2] M.F. Atiyah, *Configurations of Points*, Phil. Trans. R. Soc. Lond. A 359, 1 (2001).
- [3] R.A. Battye and P.M Sutcliffe, *Symmetric Skyrmions*, Phys. Rev. Lett. 79, 363 (1997); *Solitonic Fullerene Structures in Light Atomic Nuclei*, Phys. Rev. Lett. 86, 3989 (2001); *Skyrmions, Fullerenes and Rational Maps*, hep-th/0103026.
- [4] B. Berger, P.W. Shor, L. Tucker-Kellogg and J. King, *Local Rule-Based Theory of Virus Shell Assembly*, Proc. Natl. Acad. Sci, 91, 7732 (1994).
- [5] M.V. Berry and J.M. Robbins, *Indistinguishability for Quantum Particles: Spin, Statistics and the Geometric Phase*, Proc. R. Soc. A 453, 1771 (1997).
- [6] J.R. Edmundson, *The Distribution of Point Charges on the Surface of a Sphere*, Acta Cryst. A48, 60 (1992).
- [7] T. Erber and G.M. Hockney, *Complex Systems: Equilibrium Configurations of N Equal Charges on a Sphere*, Adv. Chem. Phys. 98, 495 (1997).
- [8] H.W. Kroto, J.R. Heath, S.C. O'Brien, R.F. Curl and R.E. Smalley,  *$C_{60}$  - Buckminsterfullerene*, Nature 318, 162 (1985).

- [9] T.W Melnyk, O. Knop and W.R. Smith, *Extremal Arrangements of Points and Unit Charges on a Sphere: Equilibrium Configurations Revisited*, Can. J. Chem. 55, 1745 (1977).
- [10] K.J. Nurmela, *Minimum-Energy Point Charge Configurations on a Circular Disk*, J. Phys. A 31, 1035 (1998).
- [11] J.J. Thomson, *On the Structure of the Atom*, Philos. Mag. 7, 237 (1904); *On the Structure of the Molecule and Chemical Combination*, Philos. Mag. 41, 510 (1921).
- [12] W.P. Thurston, *Shapes of Polyhedra and Triangulations of the Sphere*, Geometry and Topology Monographs 1, 511 (1998).
- [13] P.J.M. van Laarhoven and E.H.L. Aarts, *Simulated Annealing: Theory and Applications*, Kluwer Academic Publishers, (1987).